Contents

3 The MiniBooNE Neutrino Beam and the Magnetic Focusing Horn 1

3.1 Overview of the MiniBooNE neutrino beam 1

3.1.1 The 8 GeV neutrino beamline and the primary proton beam . 2

3.1.2 Target hall and the secondary meson beam 4

3.1.3 Decay region and the tertiary neutrino beam 6

3.2 The MiniBooNE neutrino focusing horn 7

3.2.1 Horn physics-driven requirements and design 7

3.2.2 Horn testing 13

3.2.3 Horn performance 14

Bibliography 18

Chapter 3

The MiniBooNE Neutrino Beam and the Magnetic Focusing Horn

In this Chapter, the MiniBooNE neutrino beamline is described. Section 3.1 gives a brief overview of the Fermilab 8 GeV neutrino beamline as a whole. Section 3.2 describes in more detail the MiniBooNE neutrino focusing horn, which has been the hardware project followed during the course of this thesis. Predictions on the neutrino fluxes at the MiniBooNE detector from this beamline are covered in the next Chapter.

3.1 Overview of the MiniBooNE neutrino beam

The MiniBooNE neutrino beam is a high-intensity, conventional neutrino beam produced via the decay of mesons and muons in a decay region following a target hall region, where meson production and focusing occurs. Mesons are produced in the target hall via inelastic interactions of 8 GeV kinetic energy protons from the Fermilab Booster accelerator in a thick Beryllium target, and then focused by a magnetic focusing horn surrounding the target and by a collimator system located downstream of the horn. An overview of the 8 GeV beamline, target hall, decay region and

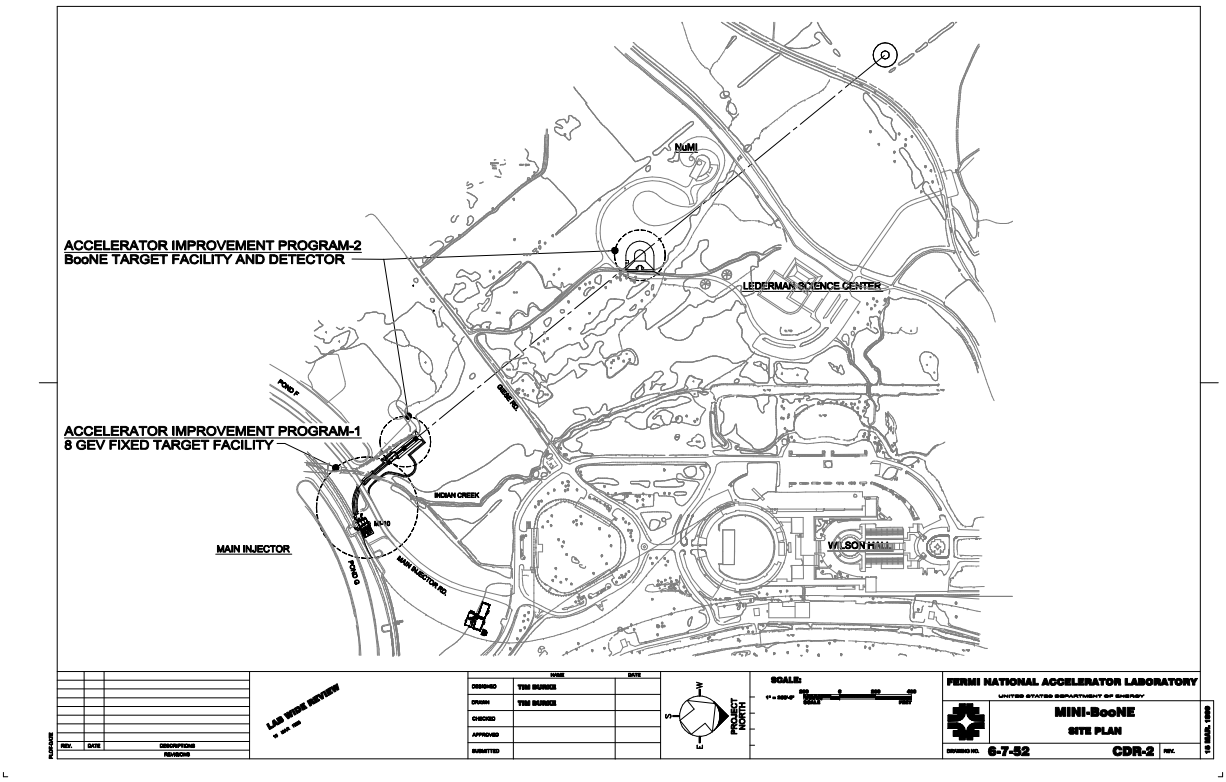

Figure 3.1: *Site map of the Fermi National Accelerator Laboratory, showing the location of the 8 GeV neutrino line, the MiniBooNE target hall, decay region, and detector.*

MiniBooNE detector locations is shown in Fig. 3.1.

3.1.1 The 8 GeV neutrino beamline and the primary proton beam

The primary beam [1, 3] uses protons accelerated to 8 GeV kinetic energy by the Fermilab Booster, and by the earlier stages in the Fermilab proton accelerator complex: the Cockroft-Walton pre-accelerator and the Linear Accelerator. Selected batches containing approximately $5 \cdot 10^{12}$ protons are extracted via a pulsed magnet in the Fermilab Main Injector tunnel, prior to further acceleration by the Main Injector, and bent by about 80 degrees toward the MiniBooNE target hall via dipole magnets. Focusing is provided by permanent and electro-magnet quadrupoles located in the 200 m long beamline section between the beam extraction location and the MiniBooNE

target location.

Particle trajectories are monitored on a pulse-by-pulse basis via a system of devices measuring the beam transverse position, direction and profile at various longitudinal positions along the beamline. An automatic beamline correction program uses the measured beam positions to correct in real-time minor deviations from the nominal beam trajectory, by adjusting the magnet settings. The typical beam alignment and divergence measured by the beam position monitors located near the target are within 1 mm and 1 mrad of the nominal target center and axis direction, respectively; the typical beam focusing on target measured by beam profile monitors is of the order of 1-2 mm (RMS) in both the horizontal and vertical directions. These parameters are well within the experiment requirements, dictated by the 5 mm in radius, 71 cm long, cylindrical beryllium target.

The number of protons delivered to the MiniBooNE target is measured for each proton batch, using a toroid located near the target along the beamline. The toroid calibration, performed on a pulse-by-pulse basis, provides a 1% accuracy on the measurement of the number of protons to MiniBooNE.

Protons that are not properly captured by the beamline optics may yield beam losses along the beam transport line, and may generate hazardous radio-activation of beamline elements, air and ground water. Therefore, several monitors measuring localized beam losses are located along the beamline. Moreover, a monitoring system measuring the total beam losses along the beamline is used, based on the difference between the measured beam intensities at the beamline initial and final locations. A beam permit system based on these (and other) inputs is used to promptly inhibit beam to the MiniBooNE target hall if abnormal conditions occur.

The readouts of beam control (*e.g.*, magnet settings) and monitoring systems (*e.g.*, beam intensity, position, and losses) are recorded and time-stamped for each proton batch, and the beam datastream is synchronized and merged with the corresponding MiniBooNE detector datastream.

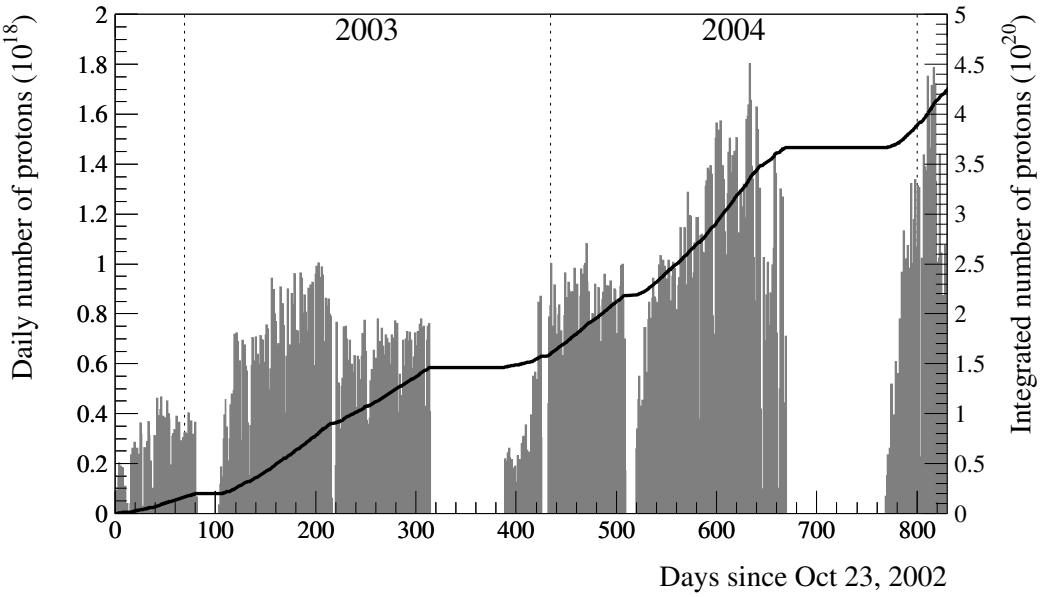

Figure 3.2: *Number of protons delivered to the MiniBooNE target in the period between October, 2002, and January, 2005. The histogram shows the daily number of protons, the solid line the integrated number of protons.*

The operation of the 8 GeV beamline has been very successful since the September 2002 start-up, with downtimes dominated by scheduled shutdowns of the accelerator complex. Over this period of time, the delivery of protons on the MiniBooNE target has been mostly dictated by the limits imposed on beam losses within the Booster accelerator, and not by losses in the 8 GeV beamline or by hardware limitations. Figure 3.2 shows the number of protons delivered to MiniBooNE since start-up: the positive trend over time in the daily number of protons is indicative of a reduction in the fraction of Booster beam losses. In the period October 2002 - January 2005, more than $4.2 \cdot 10^{20}$ protons have been delivered to MiniBooNE.

3.1.2 Target hall and the secondary meson beam

Primary protons from the 8 GeV beamline strike a thick beryllium target located in the MiniBooNE target hall. Hadronic interactions of the protons with the target material produce a beam of secondary mesons, mostly pions and Kaons. The tar-

get [2] is made of seven cylindrical slugs that are 10.2 cm in length and 0.48 cm in radius, corresponding to a total target length of 71 cm, or about 1.7 inelastic interaction lengths. The target geometry is dictated by the requirement of having a large fraction of primary protons that inelastically interact within the target, and a small fraction of reinteractions for the secondary mesons. The multi-slug design is dictated by the requirement of dealing with the thermal shock within the target due to the beam proton pulses. The target material choice, beryllium, is dictated mainly by the requirement of minimizing the radioactivity levels in the target hall due to long-lived isotopes produced by the proton beam exposure.

The target is equipped with a closed air cooling system, in order to dissipate the power $P \simeq 600$ W deposited by the primary and secondary beam in the target under normal operation ($5 \cdot 10^{12}$ protons per batch, five batches per second). The time-averaged beam heat load is efficiently removed by flowing air longitudinally along the target, at a volumetric rate of $dV/dt \simeq 8 \cdot 10^{-3}\ m^3/s$. A redundant system of radiation-hard devices monitor the air flow rates and temperatures at various locations in the target cooling system, and inhibit beam if abnormal conditions are measured. Typical measured values for the temperature of the air exiting from the target area are of the order of: $T_{out} = T_{in} + P/(c_P \rho dV/dt) \simeq 100$ degC, where $T_{in} \simeq 36$ degC is the temperature of the air coolant entering the target area, $c_P = 10^3\ J/(kg \cdot K)$ is the air specific heat at constant pressure, $\rho = 1.20\ kg/m^3$ is the air density, and P and dV/dt are defined above. Target temperatures of the order of 120 degC are inferred from the measured air temperature T_{out}, well below the temperatures that may cause permanent damage (softening) to the beryllium and aluminum materials in the target/horn system.

The beryllium target is surrounded by a magnetic focusing horn [2, 4], bending the positively-charged secondary particles that emerge from the interactions in the target along the direction pointing to the MiniBooNE detector. The focusing is produced by the toroidal magnetic field present in the air volume between the horn's two

coaxial conductors. The magnetic field is produced by current flowing along the horn inner (small radius) conductor, and back along the outer (large radius) conductor. The polarity of the horn current flow can be switched, in order to focus negatively-charged mesons, and therefore produce an anti-neutrino beam instead of a neutrino one. The heat produced in the horn inner conductor by current and by beam deposition is removed via a water cooling system. Details about the horn physics-driven requirements, mechanical and electrical design, testing, and operational performance are given in Section 3.2.

3.1.3 Decay region and the tertiary neutrino beam

The beam of focused, secondary mesons emerging from the target/horn region is further collimated via passive shielding, and allowed to decay into neutrinos in a cylindrical decay region filled with air, 50 m long and 90 cm in radius [2]. A beam absorber located at the end of the decay region stops the hadronic and muonic component of the beam, and only a pure neutrino beam pointing toward the detector remains, mostly from $\pi^+ \rightarrow \mu^+\nu_\mu$ decays. Details about the meson and muon decays occurring in the decay region that are of relevance for the MiniBooNE neutrino flux are described in the next Chapter.

The beamline design allows to reduce the length of the decay region to a half of its current length, by lowering an intermediate, movable abosrber currently located above the decay pipe, at a distance of 25 m from the target.

The decay region is also instrumented with a detector capable of measuring the momentum, energy, and charge sign of muons from the decays of kaons in the secondary beam. The muon counter consists of a muon drift pipe, subtending a 7^o angle with respect to the axis of the decay region and intersecting it 9 m upstream of the 50 m absorber, and of a collimator, spectrometer and range stack detector located near the 50 m absorber. The kinematic constraints imposed on the muons by this ge-

metrical setup allows to select the higher transverse momentum (p_t) muons produced in kaon decays, distinguishing them from the lower p_t muons from pion decays, and therefore to constrain the kaon content in the secondary beam.

3.2 The MiniBooNE neutrino focusing horn

In the following, the MiniBooNE horn is described in greater detail. The horn physics-driven requirements and design, horn testing, and horn performance are discussed.

3.2.1 Horn physics-driven requirements and design

The MiniBooNE horn design, and more generally the beamline design, are driven by the requirements for the MiniBooNE $\nu_\mu \rightarrow \nu_e$ search in the $\Delta m^2 \simeq 1\ eV^2$ range, discussed in the previous Chapter. In order to maximize the $\nu_\mu \rightarrow \nu_e$ sensitivity in the $\Delta m^2 \simeq 1\ eV^2$ range (as suggested by the LSND result), the beamline is designed to: a) provide 10^{21} protons on target in a timely manner, b) maximize the ν_μ flux at the detector between 0.3 and 1.3 GeV, c) minimize the intrinsic ν_e flux contamination in the beam, d) be operated in both neutrino and antineutrino running modes, and e) understand well the neutrino flux systematics.

The MiniBooNE horn was designed with these physics goals in mind. First, most of the design criteria for the two MiniBooNE horns built so far were dictated by the necessity to withstand an average (instantaneous) pulse repetition rate of 5 (15) Hz over a lifetime of approximately 100 million pulses at 170 kA peak horn current, to meet the proton delivery requirements (goal a)). Second, the horn geometrical shape and horn current specifications are essential factors in meeting the ν_μ flux optimization requirements (goal b)). Moreover, the horn power supply design allows to switch horn current polarity, and therefore neutrino sign selection (goal d)).

Some of the most important horn mechanical and electrical design characteristics

Material	aluminum alloy 6061-T6
Inner conductor outer radius	2.2-6.54 cm
Outer conductor inner radius	30 cm
Length	185 cm
Peak current	170 kA
Maximum magnetic field	1.5 Tesla
Current pulse duration (half-period)	140 μs
Voltage on horn	3 kV
Skin depth	1.4 mm
Average (maximum) repetition rate	5 (15) Hz
Power dissipation by ohmic losses	2.5 kW
Power dissipation by beam deposition	0.8 kW
Cooling water flow rate	1 l/s
Design lifetime	10^8 pulses in 1 year at 97.5% CL

Table 3.1: *Horn mechanical and electrical design properties.*

are listed in Tab. 3.1. The horn material is an aluminum alloy, particularly suitable for its high electrical conductivity, welding ability, resistance to corrosion, and low residual radio-activation. The geometrical shape of the horn, and in particular the shape of its inner conductor, is optimized by a full simulation for the expected neutrino fluxes at MiniBooNE. The inner conductor shape can be seen in the left panel of Fig. 3.3. The inner conductor is a 2.2 cm outer radius cylinder in the horn upstream half, while it is composed of two, larger radii (between 2.2 and 6.54 cm), intersecting cones in the horn downstream half, to avoid over-focusing of positively-charged tracks produced at small angles within the target. The total horn length of 185 cm, and the horn peak current of 170 kA, are also chosen based on simulations aimed at optimizing the MiniBooNE neutrino flux. The horn current pulse is a half-sinusoid with half-period $T/2$ of aqpproximately 140 μs, timed such that the 1.6 μs long beam spill

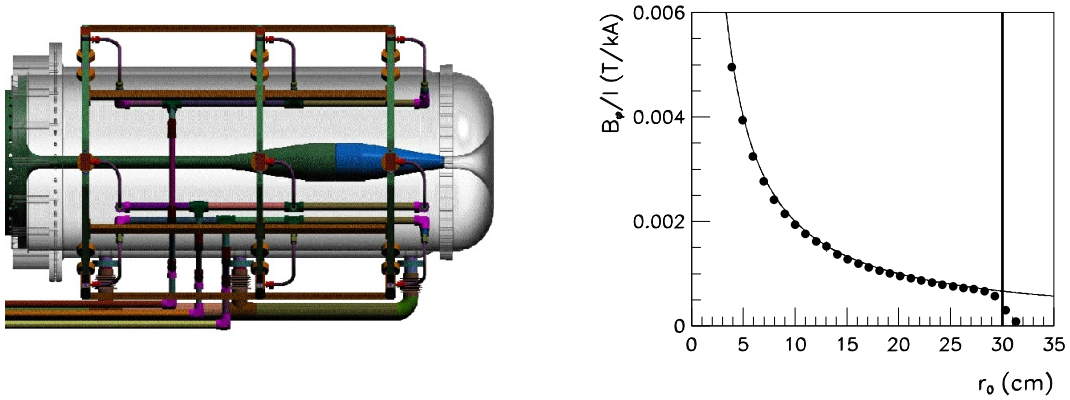

Figure 3.3: *Left: drawing of the MiniBooNE horn and its water cooling system; the horn outer conductor surface is made transparent to show the horn inner conductor shape and the target. Right: points indicate measurements of the azimuthal component of the horn magnetic field B_ϕ divided by the peak horn current I, as a function of the distance r from the horn axis. The solid line is the prediction from Eq. 3.2, and the solid vertical line is the inner radius of the horn outer conductor.*

crosses the horn/target assembly during peak horn current. Given this horn current circular frequency $\omega = 2\pi/T$, and the aluminum permeability μ and conductivity σ, the skin depth $\delta = \sqrt{2/(\mu\sigma\omega)}$ is 1.4 mm, yielding a surface magnetic field inside the aluminum inner conductor with negligible impact on the neutrino fluxes.

The horn electrical circuit and mode of operation can be described, in its simplest terms, by an under-damped LCR circuit. The energy is initially stored in a capacitor bank with capacitance C=1,344 μF, charged by the horn power supply. Beam on target triggers the capacitor bank discharge, via silicon controlled rectifiers (SCR), into the horn load. The electrical connection between the power supply and the horn is provided by four, high-current transmission lines, characterized by a planar design (striplines) in order to minimize their inductance. The horn current pulse is given by:

$$i(t) = \frac{V_0}{\omega L} e^{-\beta t} \sin \omega t \tag{3.1}$$

where $V_0 \simeq 6.0$ kV is the capacitor bank voltage corresponding to a peak horn current of 170 kA, $\beta = R/(2L)$, $\omega = \omega_0\sqrt{1-\gamma^2}$, $\omega_0 = 1/\sqrt{LC}$, $\gamma = (R/2)\sqrt{C/L}$, and

Component	Inductance (μF)	Resistance ($m\Omega$)	Power (kW)
Capacitor bank plus losses	0.37	3.00	31.0
Transmission line	0.34	0.27	2.8
Horn	0.70	0.24	2.5
Total	1.41	3.51	36.3

Table 3.2: *Resistive and inductive impedances of the various components of the horn electrical circuit, as well as power dissipation by ohmic losses for 5 Hz average repetition rate, 170 kA peak horn current operation.*

R, L are the resistive and inductive impedances of the horn circuit, summarized in Tab. 3.2. After the discharge, a separate circuit is used to recover most of the energy initially stored in the capacitor bank; the energy lost from ohmic losses is replaced by the charging power supply, in time for the next discharge cycle to begin. Under typical operations, a 15 Hz train of 5-10 horn pulses is used, interleaved by a $\simeq 2$ s hold-off time. The waveforms of the horn power supply voltage and current (including the charge recovery) can be seen in Fig. 3.4, showing one of the graphical interfaces used to monitor the horn operation.

In order to dissipate in an effective way the power deposited in the horn inner conductor by ohmic losses and beam energy loss, the MiniBooNE horn uses a water cooling system. Eighteen nozzles external to the horn outer conductor, and vibrationally isolated from the horn itself, continuously spray water on the horn inner conductor through openings in the horn outer conductor, at a flow rate of about 1 liter per second. The radioactive cooling water is kept in a closed circuit, equipped with a water to water heat exchanger to remove heat, and a filter to remove particulate content in the water.

Given this current pulse, the toroidal magnetic field between the horn inner and outer conductors at peak horn current $I_0 \simeq V_0 \exp[-\pi\beta/(2\omega)]/(\omega L)$ can be accurately approximated by the familiar expression for an infinitely long, straight conductor (in

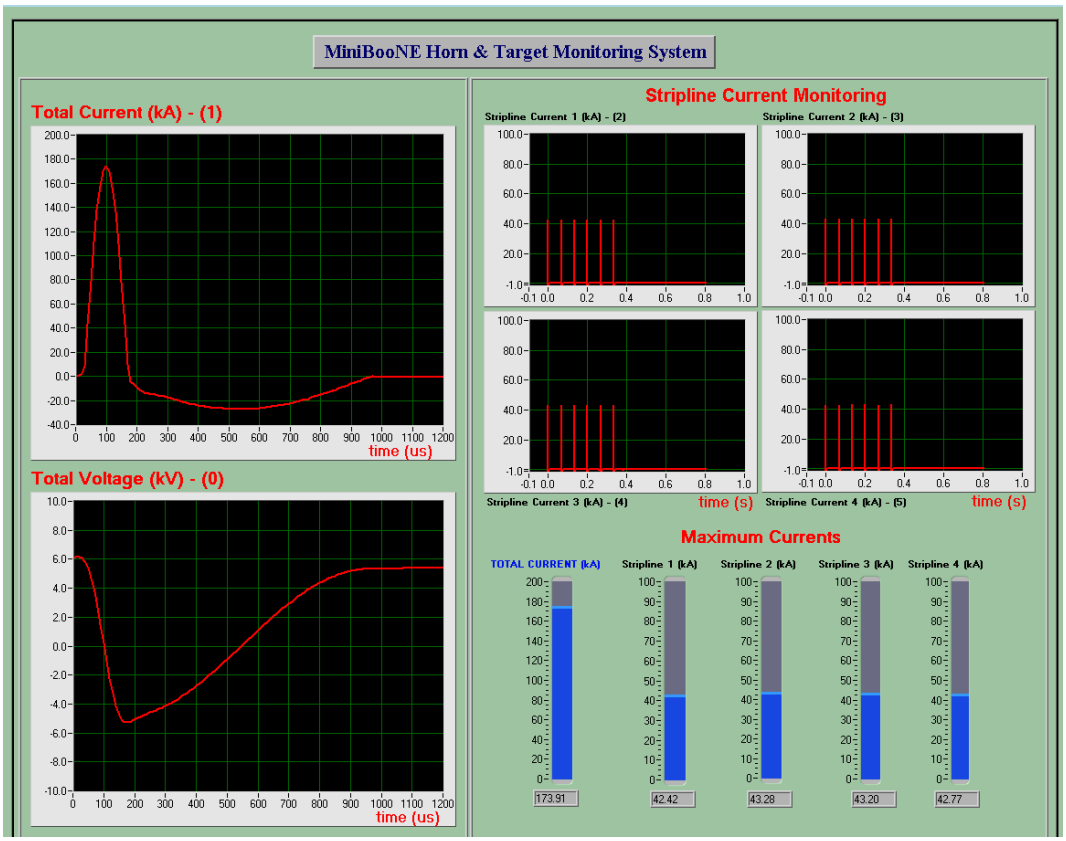

Figure 3.4: *Current and voltage waveforms at the horn power supply.*

SI units):

$$B_\phi = \frac{\mu_0}{2\pi}\frac{I_0}{r}, \;\; B_r = B_z = 0 \tag{3.2}$$

where μ_0 is the magnetic permeability of air, and r is the distance from the horn axis.

In order to quantify the performance of the MiniBooNE horn design summarized above, we define the neutrino focusing factor merit factor as:

$$\overset{(-)}{F}(E) = \frac{\phi(E; \overset{(-)}{\nu}_\mu)}{\phi_0(E; \overset{(-)}{\nu}_\mu)} \tag{3.3}$$

where $\phi_0(E; \overset{(-)}{\nu}_\mu)$ is the muon (anti)neutrino flux at the MiniBooNE detector for perfect focusing, and $\phi(E; \overset{(-)}{\nu}_\mu)$ is the corresponding flux prediction for the MiniBooNE horn in various operating modes. Perfect focusing is defined here as the neutrino flux obtained by ideally transporting on axis all electrically-charged particles reaching the downstream end of the horn, and simultaneously rotating their momentum vector to

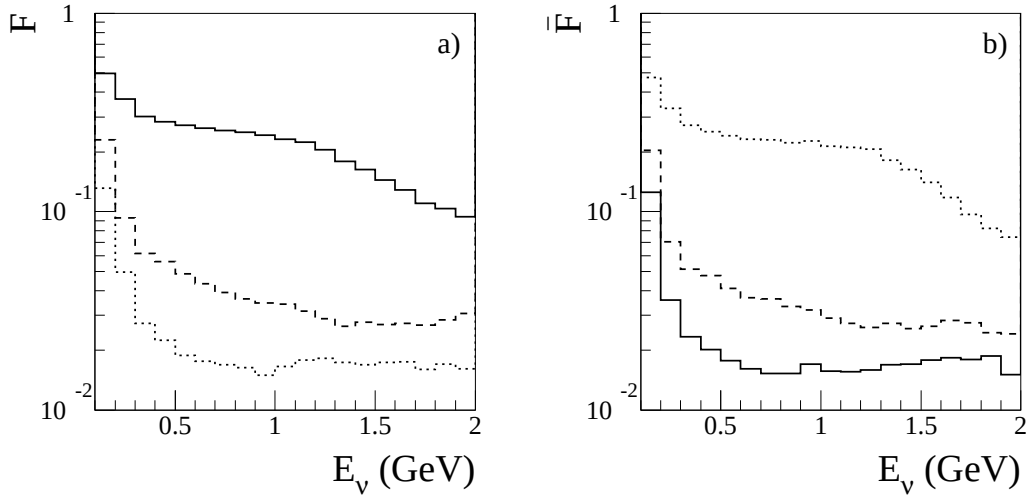

Figure 3.5: *Focusing merit factor as a function of neutrino energy E_ν of the MiniBooNE horn for muon neutrinos (a)) and muon antineutrinos (b)), expressed as fraction of flux at the MiniBooNE detector for perfect neutrino focusing. The solid, dashed, dotted lines are for neutrino, horn-off, and antineutrino running modes, respectively.*

be at zero angle with respect to the beam axis. The horn operating conditions that are simulated here to quantify the horn performance are: neutrino running mode (+170 kA peak horn current), horn-off running mode (zero horn current), and antineutrino running mode (-170 kA peak horn current). The convention for the horn current flow taken here is such that a positive horn current corresponds to a current flowing along the horn inner conductor and then back along the outer conductor, thereby focusing positively-charged tracks.

The horn performance is evaluated with a full GEANT4 simulation of the MiniBooNE target/decay region that includes all physics processes relevant for neutrino production. This simulation is described in detail in the next Chapter. The MiniBooNE horn design is very effective in boosting the $\overset{(-)}{\nu}_\mu$ flux at the MiniBooNE detector, and in selecting either a neutrino or an antineutrino beam. Specifically, for typical muon neutrino energies of $0.7 < E_\nu < 0.8$ GeV, the horn neutrino merit factor in neutrino running is predicted to be about one quarter, about six times higher than the neutrino merit factor in horn-off running (see Fig. 3.5a); a similar merit factor

is predicted for antineutrinos in antineutrino running (see Fig. 3.5b). Moreover, the merit factor for "wrong sign" neutrinos (*e.g.* antineutrinos in neutrino running) is about two times smaller than the corresponding factor in horn-off running, in the same neutrino energy range.

3.2.2 Horn testing

Prior to installation in the beamline, each of the two horns built so far for the MiniBooNE experiment has been thoroughly tested. Tests include magnetic field, mechanical vibration, and cooling measurements, as well as a fatigue test.

A map of the horn magnetic field has been measured in more than 300 locations using an inductive coil [5]. In a cylindrical coordinate system (z, φ, r) with respect to the horn axis, the measurements show no significant dependence of the nonzero azimuthal component of the field as a function of the z and φ positions within the horn field region, while the expected $1/r$ radial dependence of the field is confirmed in the explored radial range, 3.9 cm $< r <$ 30 cm, as shown in the right panel of Fig. 3.3. Moreover, the measured longitudinal component of the field is consistent with zero, given the coil alignment accuracy achieved in the measurements.

Detailed simulations and measurements of the horn vibrational response to high-current pulses were also performed, and the impact of the horn mechanical stresses on the horn lifetime were evaluated. The studies allowed to optimize material thicknesses throughout the horn, in order to ensure adequate horn lifetime, while keeping to a minimal level the impact of particle interactions in aluminum on neutrino fluxes. The vibrational measurements indicated that, despite the high repetition rate, no pileup of horn vibrational modes from one current pulse to another occur.

The necessary water cooling flow rate was determined experimentally, by measuring the heat transfer coefficient from aluminum to water for spray cooling, in a test setup with a geometry identical to the MiniBooNE horn one. In the test

setup, the inner conductor was simulated with an electrically heated tube simulating the horn inner conductor withstanding power deposition by electric current and beam. A water flow rate of the order of 1 l/s was measured to provide the necessary, $> 3000\ W/(m^2\text{degC})$, heat transfer coefficient.

Finally, each MiniBooNE horn has successfully been subject to a fatigue test, consisting in pulsing the horn in nominal conditions (5 Hz average repetition rate, 170 kA peak horn current), for a total of 10 million current pulses.

3.2.3 Horn performance

Over the period between September, 2002, and January, 2005, more than 10^8 proton batches were delivered from the Booster accelerator to the MiniBooNE target hall, with each proton batch triggering a 170 kA peak current pulse on the MiniBooNE horn. The daily average repetition rate and the integrated number of horn pulses, as a function of time, are shown in Fig. 3.6.

As discussed above, the horn repetition rate over this running period has been determined mostly by the FNAL Booster accelerator mode of operation. In particular, the radiation concerns due to proton losses in the Booster did not permit to pulse the horn at the design average repetition rate of 5 Hz throughout the run; the design repetition rate has been approached in recent operation. In the summer of 2004, approximately one month before a three-month long scheduled shutdown of the accelerator complex, the first MiniBooNE horn failed after $8.5 \cdot 10^7$ pulses due to a ground fault. The MiniBooNE horn/target assembly was successfully replaced during the summer 2004 shutdown, and the second horn has been pulsed more than $1.5 \cdot 10^7$ since then.

The stability of horn operation over time has also been investigated, and proved to be sufficiently reliable. The most important horn parameter to monitor in relation to physics analyses is the peak horn current. Fig. 3.7 shows the daily average peak

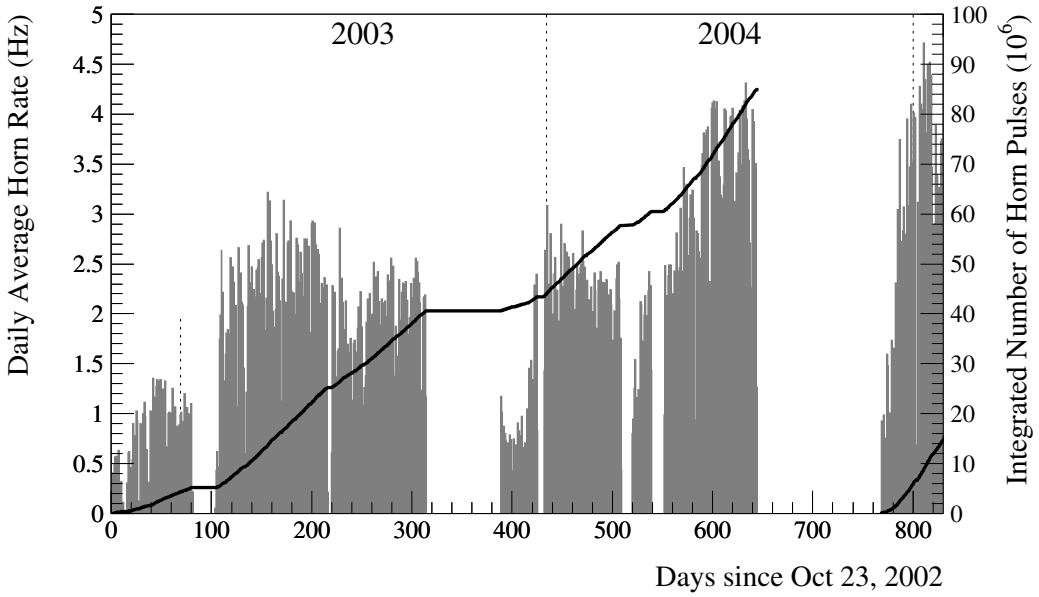

Figure 3.6: *Performance of the MiniBooNE horn in the period between October, 2002, and January, 2005. The histogram shows the daily average horn repetition rate, the solid line the integrated number of horn pulses. In the Figure, the integrated number of pulses has been reset to zero after the horn replacement.*

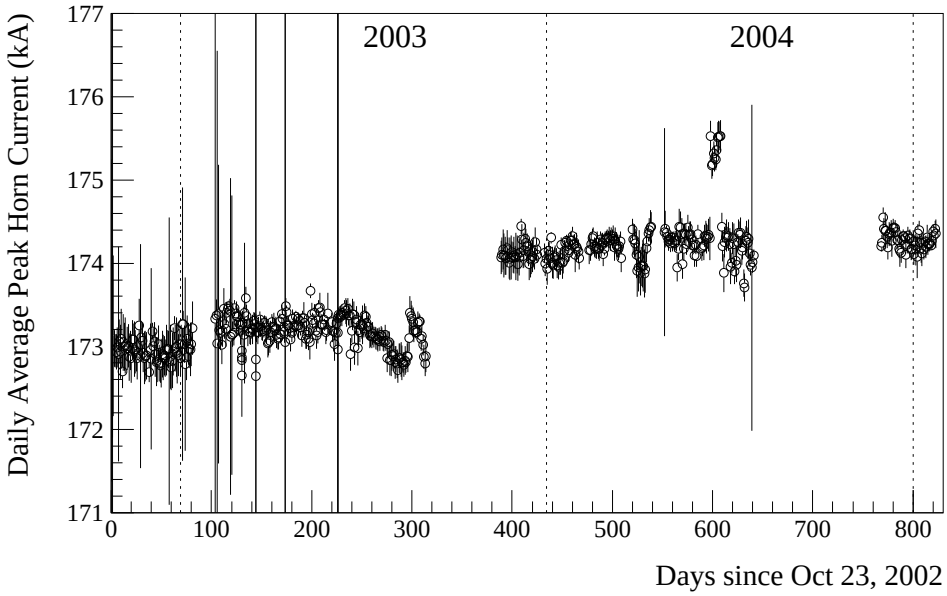

Figure 3.7: *Performance of the MiniBooNE horn in the period between October, 2002, and January, 2005. The points and error bars show the mean and the RMS of the peak horn current averaged over one day.*

horn current obtained by averaging over all horn pulses in the day. Over the more than two years of operation, the peak horn current has not changed by more than 1%. It is estimated that a 1% variation in the peak horn current would cause only a 0.7% variation in the neutrino flux at the MiniBooNE detector.

In Section 3.2.1, we have described the expected focusing performance of the MiniBooNE horn as a function of neutrino energy, expressed in terms of fraction of perfect focusing neutrino flux. In this section, we discuss the measured rates of neutrino candidate events in the MiniBooNE detector per proton on target, for both horn-on, neutrino running mode, and horn-off mode.

MiniBooNE neutrino candidates are defined here in a very simple way, using exclusively MiniBooNE PMT hit multiplicity and timing, and no event reconstruction. Details on the MiniBooNE detector are given in Chapter 6, and only the detector aspects necessary to define neutrino candidates in this context are explained below. The sample of neutrino candidates is triggered by beam on target, and uses the information on the PMT charges and times in the detector recorded over a 19.2 μs time interval. Next, the PMT activity is split into subevents, defined as clusters of time-related PMT hits of a typical duration of about 100 ns. The event splitting algorithm is introduced to tag the delayed light produced by electrons from muon decays, generally occurring several hundreds of nanoseconds after the neutrino interaction; the presence of electrons from muon decays in the detector generally cause the event to be split in > 1 subevents. The simple neutrino event selection applied here requires less than 6 PMT hits in the veto region for the first subevent in the event, in order to reject cosmic ray muons crossing the detector in coincidence with beam activity. Moreover, the PMT hit multiplicity in the main detection region for the first subevent is required to be greater than 200, in order to reject the < 52.3 MeV electrons produced by the decays-at-rest of cosmic ray muons occurring before the 19.2 μs-long beam window. Overall, this simple event selection ensures a signal-to-background ratio in excess of 1000, where "signal" indicates here a neutrino-induced event, while

Running Mode	$N_{\rm pot}$	N_ν	$N_\nu/N_{\rm pot}$
Horn-on Neutrino	$1.95 \cdot 10^{20}$	$218,337$	$1.120 \cdot 10^{-15}$
Horn-off	$1.11 \cdot 10^{19}$	$2,033$	$0.184 \cdot 10^{-15}$

Table 3.3: Number of protons on target $N_{\rm pot}$, number of neutrino candidate events N_ν, and ratio of neutrino candidate events to protons on target $N_\nu/N_{\rm pot}$, for selected periods of horn-on neutrino running mode and for horn-off running mode.

"background" any other source of PMT activity in the MiniBooNE detector.

The number of protons on target are estimated from the readout of the toroid located immediately upstream of the MiniBooNE target, as discussed in Section 3.1.1. Moreover, beam quality cuts are applied to ensure that the protons hit the target, the horn fires, and that the toroid readout does not differ in a significant way from additional beam instrumentation located in the Booster neutrino beamline.

Table 3.3 shows the number of protons on target, the number of neutrino candidate events, and the neutrino-to-proton ratio measured in MiniBooNE in both horn-on and horn-off configurations over the running period October, 2002, to April, 2004. Most of the run time has been spent in horn-on, neutrino mode; two weeks were devoted to horn-off running mode in April, 2004. We observe a 6-fold increase in the neutrino candidate event rate per proton on target, $N_\nu/N_{\rm pot}$ in Tab. 3.3, by operating the horn in neutrino running mode, compared to horn-off mode.

This boost in neutrino interaction rate due to the horn focusing is crucial in order to accomplish the main physics goal of the MiniBooNE experiment discussed in Chapter 1, that is a $\nu_\mu \rightarrow \nu_e$ oscillation measurement with sufficient sensitivity in the neutrino mass and mixing parameter space indicated by the LSND signal. As mentioned in the previous Chapter, the MiniBooNE $\nu_\mu \rightarrow \nu_e$ sensitivity is dominated by the statistical uncertainty on the number of neutrino candidates, and therefore a 6-fold increase in neutrino rate roughly corresponds to a $\sqrt{6}$ increase in sensitivity.

Bibliography

[1] I. Stancu *et al.* [MiniBooNE collaboration], "Technical Design Report for the 8 GeV Beam,"
http://www-boone.fnal.gov/publicpages/8gevtdr_2.0.ps.gz

[2] I. Stancu *et al.* [MiniBooNE collaboration], "Technical Design Report for the MiniBooNE Neutrino Beam,"
http://www-boone.fnal.gov/publicpages/target_tdr.ps.gz

[3] C. Moore *et al.*, "Initial Operation of the Fermilab MiniBooNE Beamline", Proceedings of the 2003 Particle Accelerator Conference,
http://accelconf.web.cern.ch/AccelConf/p03/PAPERS/TPPB013.PDF

[4] http://www.bartoszekeng.com/mboone/mboone.htm

[5] L. Bugel and M. Sorel, "Magnetic Field Measurements for the MiniBooNE Prototype Horn", BooNE Technical Note 34 (2001);